AGU PUBLICATIONS

Geophysical Research Letters

RESEARCH LETTER
10.1002/2017GL073580

Key Points:
- Coseismic ground deformation of the 2016 Central Italy earthquake sequence measured with InSAR and GPS data
- At least four main normal fault segments played an active role in the sequence
- Antithetic faults and/or preexisting compressional structures may have been reactivated during the sequence with extensional kinematics

Supporting Information:
- Supporting Information S1

Correspondence to:
V. De Novellis,
denovellis.v@irea.cnr.it

Citation:
Cheloni, D., et al. (2017), Geodetic model of the 2016 Central Italy earthquake sequence inferred from InSAR and GPS data, *Geophys. Res. Lett.*, *44*, 6778–6787, doi:10.1002/2017GL073580.

Received 24 MAR 2017
Accepted 5 JUL 2017
Accepted article online 6 JUL 2017
Published online 15 JUL 2017

©2017. The Authors.
This is an open access article under the terms of the Creative Commons Attribution-NonCommercial-NoDerivs License, which permits use and distribution in any medium, provided the original work is properly cited, the use is non-commercial and no modifications or adaptations are made.

Geodetic model of the 2016 Central Italy earthquake sequence inferred from InSAR and GPS data

D. Cheloni[1], V. De Novellis[2], M. Albano[1], A. Antonioli[1], M. Anzidei[1], S. Atzori[1], A. Avallone[1], C. Bignami[1], M. Bonano[2], S. Calcaterra[3], R. Castaldo[2], F. Casu[2], G. Cecere[1], C. De Luca[2], R. Devoti[1], D. Di Bucci[4], A. Esposito[1], A. Galvani[1], P. Gambino[3], R. Giuliani[4], R. Lanari[2], M. Manunta[2], M. Manzo[2], M. Mattone[4], A. Montuori[1], A. Pepe[2], S. Pepe[2], G. Pezzo[1], G. Pietrantonio[1], M. Polcari[1], F. Riguzzi[1], S. Salvi[1], V. Sepe[1], E. Serpelloni[1], G. Solaro[2], S. Stramondo[1], P. Tizzani[2], C. Tolomei[1], E. Trasatti[1], E. Valerio[5], I. Zinno[2], and C. Doglioni[1,5]

[1]Istituto Nazionale di Geofisica e Vulcanologia, Rome, Italy, [2]Istituto per il Rilevamento Elettromagnetico dell'Ambiente-Consiglio Nazionale delle Ricerche, Naples, Italy, [3]Istituto Superiore per la Protezione e la Ricerca Ambientale, Rome, Italy, [4]Dipartimento della Protezione Civile, Rome, Italy, [5]Dipartimento di Scienze della Terra, Università degli Studi di Roma "La Sapienza", Rome, Italy

Abstract We investigate a large geodetic data set of interferometric synthetic aperture radar (InSAR) and GPS measurements to determine the source parameters for the three main shocks of the 2016 Central Italy earthquake sequence on 24 August and 26 and 30 October (M_w 6.1, 5.9, and 6.5, respectively). Our preferred model is consistent with the activation of four main coseismic asperities belonging to the SW dipping normal fault system associated with the Mount Gorzano-Mount Vettore-Mount Bove alignment. Additional slip, equivalent to a M_w ~ 6.1–6.2 earthquake, on a secondary (1) NE dipping antithetic fault and/or (2) on a WNW dipping low-angle fault in the hanging wall of the main system is required to better reproduce the complex deformation pattern associated with the greatest seismic event (the M_w 6.5 earthquake). The recognition of ancillary faults involved in the sequence suggests a complex interaction in the activated crustal volume between the main normal faults and the secondary structures and a partitioning of strain release.

1. Introduction

The 2016 Central Italy earthquake sequence started on 24 August with a M_w 6.1 event, striking a sector of the Apennines (Figure 1) characterized by high geodetic strain rates [*D'Agostino*, 2014] and causing ~300 casualties and extensive damage to the town of Amatrice and surroundings. The following seismic sequence was characterized by numerous aftershocks located southeast and northwest of the epicenter [*Chiaraluce et al.*, 2017], which decreased in frequency and magnitude until the end of October, when a M_w 5.9 event occurred on 26 October about 25 km to the NW of the previous main shock, between Visso and Ussita villages (Figure 1). Moreover, on 30 October, a third large event of magnitude M_w 6.5 nucleated below the town of Norcia, striking the area between the two preceding events and filling the gap between the previous ruptures. Fault plane solutions for the main events exhibit normal faulting (http://cnt.rm.ingv.tdmt) consistent with the direction of active extension of ~3–4 mm/yr in this sector of the Apennines [*Petricca et al.*, 2015; *Devoti et al.*, 2017]. Previous geological studies [*Boncio et al.*, 2004; *Galli et al.*, 2008; *Pizzi and Galadini*, 2009] have identified several NW-SE trending normal fault systems, which are active in this area, and are often segmented by preexisting tectonic structures inherited from the pre-Quaternary compressional tectonic phases [*Pizzi and Galadini*, 2009]. However, the influence of these preexisting structures on the propagation and segmentation of the active normal faults is still not clear.

Here we exploit a large data set of interferometric synthetic aperture radar (InSAR) and GPS measurements to investigate the ground displacement field and to determine, by using elastic dislocation modeling, the geometries, and slip distributions of the causative normal fault segments associated with the three main events of the seismic sequence. To examine the achieved results, we also exploit the information on the relocated aftershocks distribution [*Chiaraluce et al.*, 2017] and on the known geologic structures of the area [*Lavecchia et al.*, 2016].

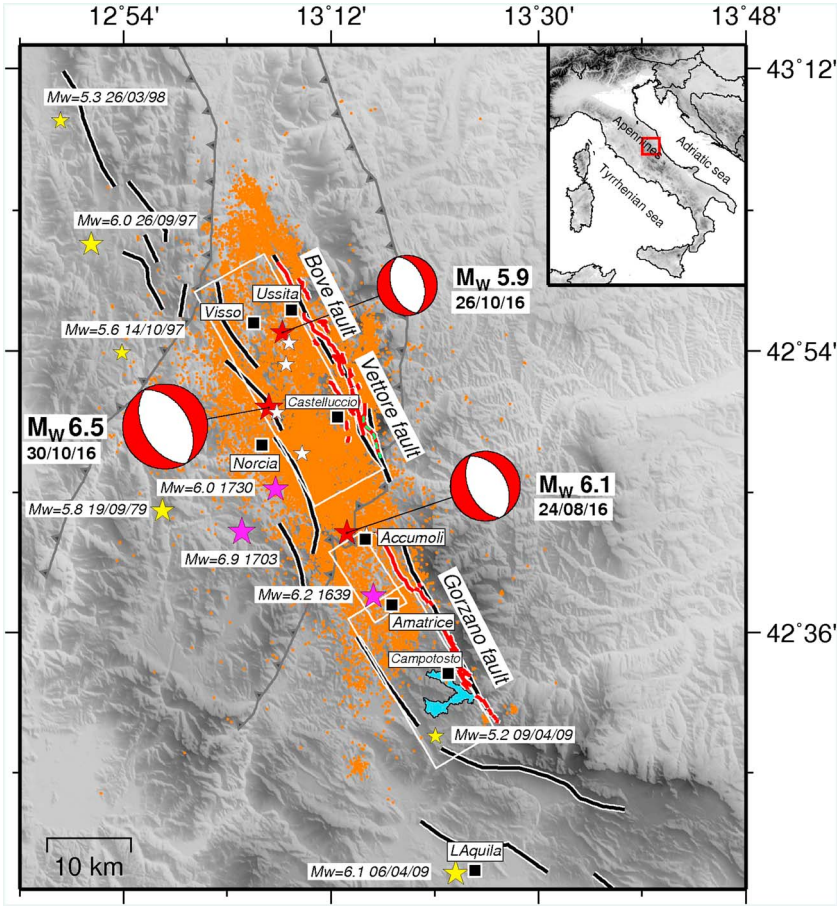

Figure 1. Seismotectonic framework of the study area. Solid black lines are the major active faults of the area [*Boncio et al.*, 2004; *Galli et al.*, 2008; *Pizzi and Galadini*, 2009], while the red ones represent the MGVB fault system, with the associated seismogenic sources (white boxes [*Falcucci et al.*, 2016]). The gray barbed lines mark the preexisting compressional front [*Pizzi and Galadini*, 2009]. Green dashed lines represent the observed surface breaks after the 24 August event [EMERGEO Working Group, 2016]. Seismicity: orange dots are relocated aftershocks [*Chiaraluce et al.*, 2017]; red stars represent the three largest shocks (moment tensor solutions from *Scognamiglio et al.* [2009]), while the white stars are $M_w > 5$ earthquakes. Previous events: purple stars show the location of historical earthquakes [*Rovida et al.*, 2011]; yellow stars show the major instrumental events [*Castello et al.*, 2006] (ISIDe: http://iside.rm.ingv.it).

2. Geodetic Data

2.1. InSAR Data

We used InSAR data acquired by different satellites (Figure S1 and Table S1 in the supporting information), provided within the emergency activities of the Italian National Service of Civil Protection. In particular, we exploited two ascending and three descending interferograms, which involve the ALOS-2, the Sentinel-1 (S1), and the COSMO-SkyMed (CSK) sensors, to measure the ground displacement due to the 24 August M_w 6.1 Amatrice earthquake and two ALOS-2 interferograms to investigate the cumulative displacement pattern relative to the 26 October M_w 5.9 Visso and the 30 October M_w 6.5 Norcia earthquakes. Moreover, an additional ascending ALOS-2 interferogram, relevant only to the Norcia event, was also used (Figure S2; see supporting information for processing strategies).

The ground deformations retrieved from the five unwrapped interferograms, including the 24 August main shock (Figure 2), are characterized by two NNW-SSE striking deformation lobes located to the west of the Mount Gorzano-Mount Vettore-Mount Bove (MGVB) alignment, with a maximum negative LOS (line of sight) displacement value of ~20 cm (negative LOS values represent increasing distances from the satellite), having a dominantly vertical component, in agreement with previous studies [*Bignami et al.*, 2016; *Lavecchia et al.*, 2016; *Huang et al.*, 2017].

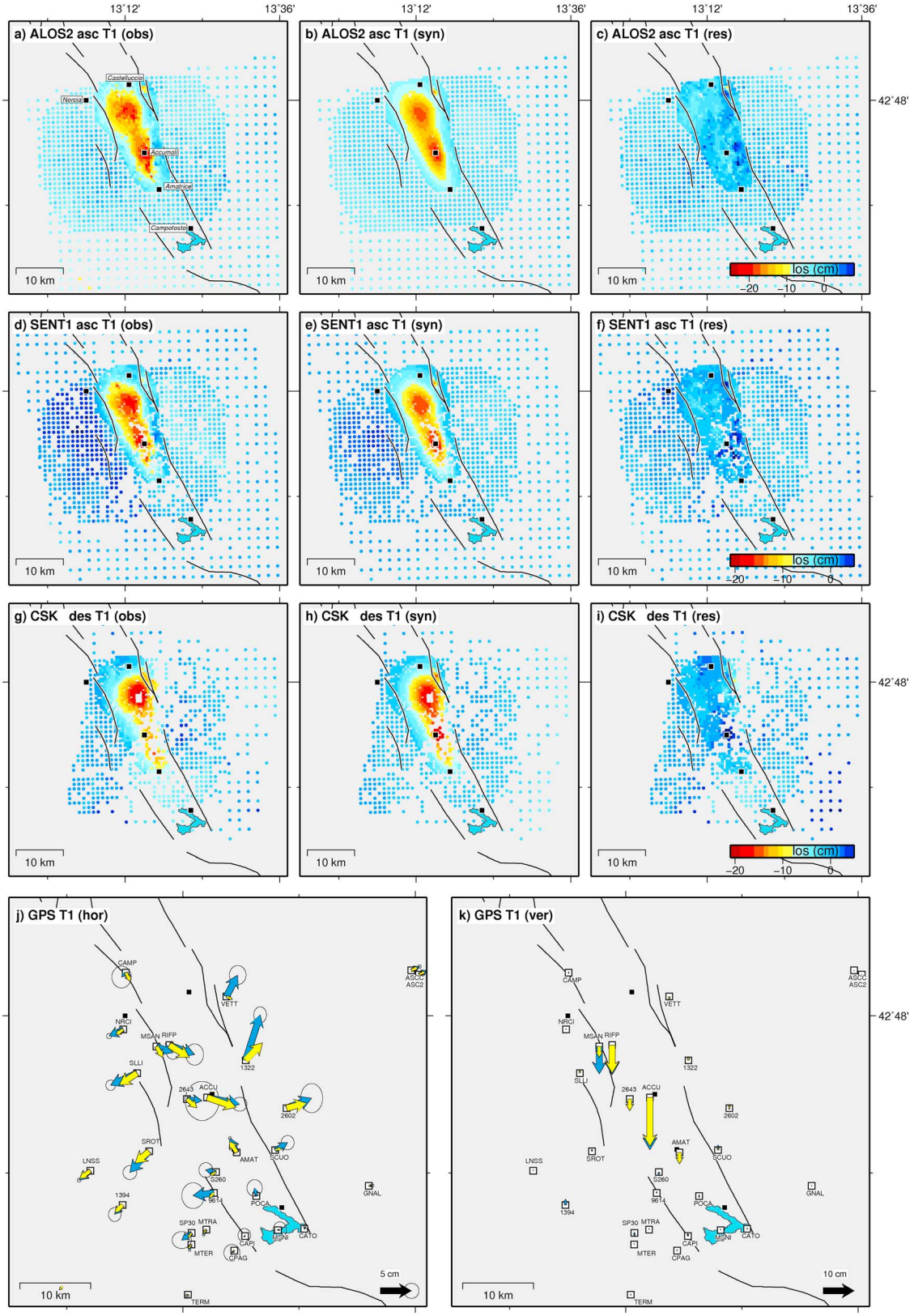

Figure 2. Geodetic displacements for the 24 August earthquake. Data, model, and residuals from the unwrapped (a–c) ALOS-2 and (d–f) S1 ascending tracks and from the (g–i) CSK descending track interferograms (the complete set of interferograms used in the inversion are provided in the supporting information). Observed (blue) and predicted (yellow) GPS (j) horizontal and (k) vertical displacements.

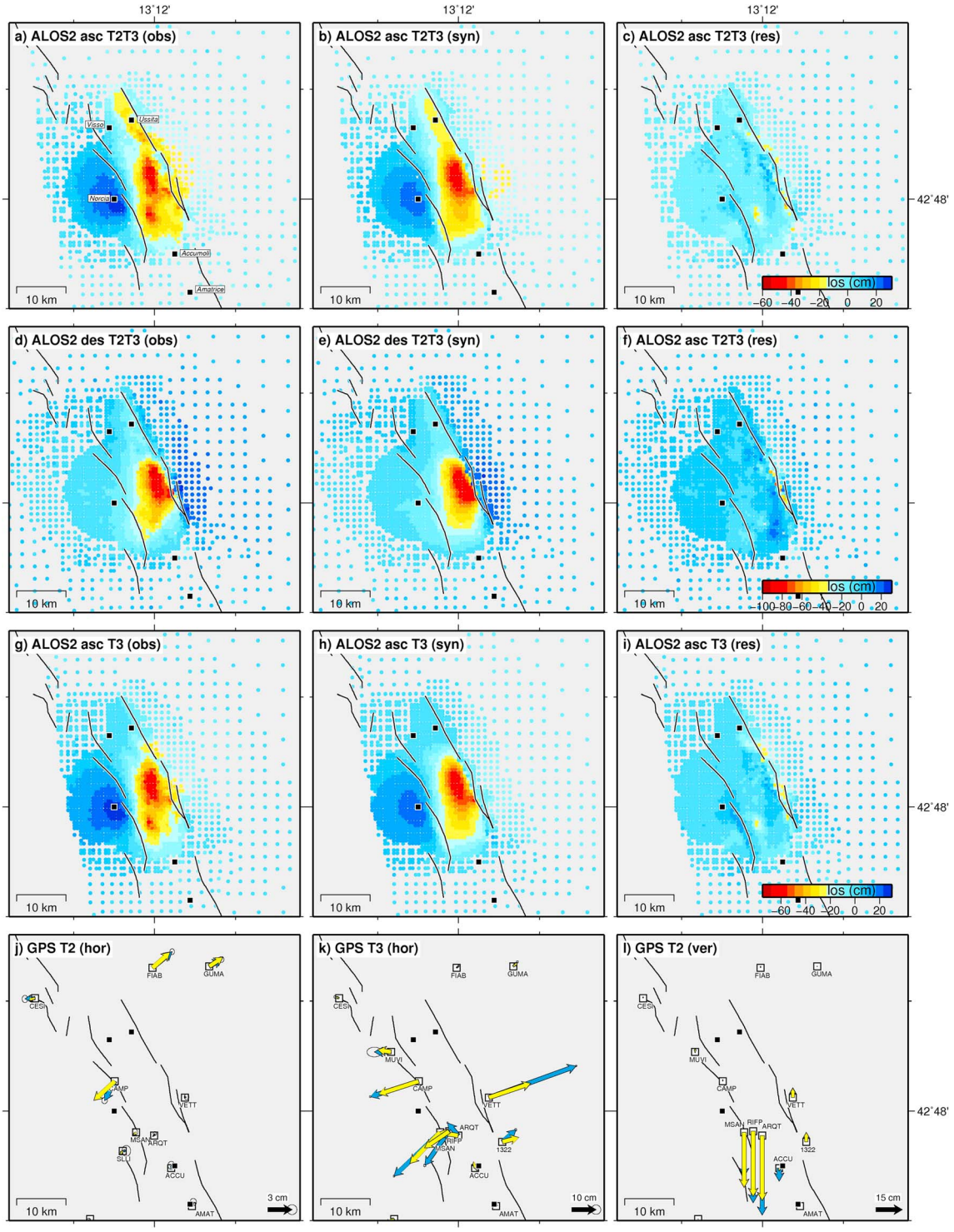

Figure 3. Geodetic displacements for the 26 and 30 October earthquakes. Data, model, and residuals from the unwrapped ALOS-2 interferograms showing the cumulative displacements from the (a–c) ascending, (d–f) descending tracks, and (g–i) the displacement field relative to the 30 October earthquake alone. (j–l) Observed (blue) and predicted (yellow) GPS horizontal displacements relative to the 26 (Figure 3j) and 30 (Figures 3k and 3l) October events, respectively. The vertical displacements are showed only for the latter event (Figure 3l).

As regards the two ALOS-2 interferograms, spanning both the 26 and 30 October earthquakes (Figure 3), they were also properly combined to retrieve the vertical and the E-W displacement components (Figure S3). Our analysis reveals a subsidence pattern extending 35 km along the NNW-SSE direction, with a local minimum

displacement of ~30 cm in correspondence to Ussita (close to the 26 October event), and a maximum detected subsidence of ~90 cm in the surroundings of Castelluccio; a slight uplift of ~15 cm was instead observed in correspondence to Norcia (Figures 3 and S3c). The E-W displacement map (Figure S3d) shows a westward movement of the Norcia area and eastward displacements of the footwall of the main normal fault system. Localized westward motions close to Castelluccio were also detected (reaching up to ~60 cm).

2.2. GPS Data

The earthquake sequence occurred where several continuous and survey mode GPS networks were operating (Figure S4). In particular, several instruments were installed at geodetic benchmarks belonging to the Istituto Nazionale di Geofisica e Vulcanologia (INGV), CaGeoNet [*Galvani et al*., 2012], and to the Istituto Geografico Militare networks. Moreover, a new INGV continuous station was built at Arquata del Tronto (see supporting information for processing strategies).

While the few coseismic offsets for the 24 August main shock derived from continuous GPS data have been already described in *Cheloni et al*. [2016] and in *Huang et al*. [2017], the complete set of GPS displacements, from both permanent and survey mode stations, are presented here for the first time. The complex coseismic deformation pattern highlights a general SW-NE oriented extension (Figures 2j and 2k), in agreement with the deformation field depicted by the InSAR measurements. The maximum displacements are ~17 cm of subsidence near Accumoli (ACCU) and ~5 cm of horizontal movement toward southeast and southwest at stations ACCU, RIFP, and SLLI (Figure 2j), respectively.

Figures 3j–3l show coseismic displacements related to the 26 and 30 October main shocks. Due to a more limited number of GPS observations with respect to the Amatrice event, both the displacement fields (Figures 3j and 3k) show a sparser displacement pattern, characterized by a general SW-NE oriented extension in different portions of the MGVB fault system. For 26 October event, the maximum horizontal displacements were observed at stations FIAB and CAMP, which moved ~3 cm toward northeast and southwest, respectively (Figure 3j), while no significant vertical patterns were observed. As regards the 30 October earthquake, the largest horizontal displacements were observed at stations VETT and MSAN, with ~40 cm of movement toward northeast and ~25 cm toward southwest, respectively (Figure 3k). The largest vertical displacements were measured at sites RIFP, MSAN, and ARQT, with a subsidence reaching up to ~20–40 cm (Figure 3l). Finally, both stations 1322 and VETT, located on the footwall of the main normal fault system, showed an uplift of ~2–5 cm.

3. Geodetic Modeling

We performed the geodetic modeling using rectangular dislocations in an elastic, homogeneous, and isotropic half-space [*Okada*, 1985]. Because the earthquake sequence occurred along the steep topographic gradient of the MGVB alignment (Figure 1), we have properly accounted for the elevation of each data point [*Williams and Wadge*, 1998]. The source modeling was carried out with a standard two-step procedure [*Atzori et al*., 2009]: a nonlinear optimization of the fault geometry with assumed uniform slip, followed by a linear slip distribution inversion on the fault with optimized fixed geometry, subdivided into patches with increasing size with depth [*Cheloni et al*., 2016]. Before modeling, the interferograms were downsampled using a resolution-based resampling technique [*Lohman and Simons*, 2005]. Additional terms (i.e., linear ramp for InSAR displacements) were also included in the inversion, to minimize the effect on the solution of any residual long-wavelength orbital signal in InSAR maps [*Pepe et al*., 2011], and a relative weight was applied to properly combine the different data sets (Figure S5). We regularize the inversion by applying positivity and smoothing (using the Laplacian operator) constraints, choosing the scalar weighting factor by examining a trade-off curve of misfit function versus solution roughness (Figure S6). Finally, resolution tests have been performed (Figures S7a and S7j) to assess which features of the slip distributions are robustly determined from the data.

3.1. The 24 August Amatrice Earthquake

The fault geometry of the source responsible for the 24 August earthquake has already been investigated by inverting geodetic [*Bignami et al*., 2016; *Cheloni et al*., 2016; *Lavecchia et al*., 2016; *Huang et al*., 2017] and seismological [*Tinti et al*., 2016; *Liu et al*., 2017] data. Compared with the previous studies, we used an augmented geodetic data set, consisting of five InSAR interferograms and of the full set of GPS displacements. The best

fitting uniform slip model consists, from north to south, of two distinct ~40° and ~50° SW dipping fault segments located beneath the two observed lobes of deformation, in agreement with hypocentral location, aftershocks distribution, and previous geodetic solutions [*Lavecchia et al*., 2016; *Huang et al*., 2017]. The data are well reproduced (Figures 2 and S8) but for the local deformation pattern depicted in all the interferograms on the western flank of the Mount Vettore and the GPS VETT on the footwall of the main fault. Despite that the InSAR local deformation has been explained both as due to a triggered landslide [*Huang et al*., 2017] and to a combination of primary faulting and gravitational phenomena [*Albano et al*., 2016], the GPS VETT offset is compatible assuming some very shallow slip on the Mount Vettore Fault. The variable slip model shows two well-separated major asperities with peaks of slip of ~1.0 and 1.4 m for the southern and northern segments, respectively (Figure 4a). The position of the main shock relative to the retrieved slip distribution supports the seismological inference of a bilateral rupture directivity [*Tinti et al*., 2016; *Bonini et al*., 2016; *Liu et al*., 2017]. The overall seismic moment of the two fault segments is 2.12×10^{18} Nm, corresponding to a M_w 6.2 earthquake.

3.2. The 26 and 30 October Visso and Norcia Earthquakes

The results of the inversion for slip distribution on the two fault planes corresponding to the activated segments of Mount Vettore-Mount Bove normal fault system were obtained from the exploitation of a geodetic data set consisting of three ALOS-2 interferograms and of the GPS coseismic offsets for the 26 and 30 October events (Figures S9–S11). In the modeling, the fault geometries were based on field data [*Falcucci et al*., 2016], focal parameters (http://cnt.rm.ingv.tdmt), and relocated aftershocks [*Chiaraluce et al*., 2017], along with the general strike of the MGVB alignment. Two fault planes were considered, with ~160° strike and 20×4 km^2 size, which compose a 40 km long tectonic structure capturing almost the whole area affected by the October seismic sequence. We tested the sensitivity of the RMS of the residuals to the overall fault dip by performing a number of inversions varying the dip (within a range of 30°–60°) of the assumed fault planes. The retrieved data are consistent with a fault dip of ~40°, in agreement with previous findings by *Lavecchia et al*. [2016] and *Huang et al*. [2017] for the southern sector of the causative Mount Vettore Fault. We subdivided the fault planes into small patches, solving for slip and rake values on each patch. At shallow depth fault patches are about 1×1 km^2 wide, while the deeper ones are approximately 3.5×3.5 km^2. Our preferred model satisfactorily reproduces the main characteristic of both the observed InSAR and GPS displacements (Figure S9). Our model (Figure S10) highlights that the 26 October event occurred on the northern segment of the MGVB fault system, releasing a seismic moment of 1.97×10^{18} Nm, equivalent to a M_w 6.16 earthquake. The slip pattern shows a single main coseismic asperity on the southeastern portion of the fault plane, with peak slip of ~0.8 m (Figures S10 and S11). For the 30 October main shock, our model retrieves slip on the Mount Vettore Fault, which releases a seismic moment of 8.46×10^{18} Nm, equivalent to a M_w 6.59 earthquake. Most of the coseismic slip occurred on one main asperity (up to >2 m of slip) located updip of the hypocenter, between 3 and 7 km depth (Figures S10 and S11). In addition, some slip (up to ~1 m) is also required in the shallower portion of the plane, in correspondence to the observed surface breaks [*Galadini et al*., 2017], and in the deeper southeastern part of the fault, below the main coseismic asperity of the 24 August event, which ruptured only a portion of the Mount Vettore Fault. Our results are in agreement with the preliminary findings from *INGV Working Group "GPS Geodesy"* [2016] and *Liu et al*. [2017].

Moreover, our results revealed that the assumption of slip occurring only on the two segments of the SW dipping MGVB fault system generates some displacement residuals (up to ~10 cm) in the 30 October coseismic interferograms, especially in the area of Norcia (Figure S9). In order to better explain the displacement field imaged by these ALOS-2 interferograms, we hypothesized the occurrence of a further amount of slip on a secondary fault and explored two different hypotheses: (1) an antithetic NE dipping normal fault emerging in the Norcia area and well visible in the relocated aftershocks distribution (Figures 4g and 4i) and (2) a preexisting low-angle WNW dipping thrust segment below the Castelluccio plain (Figures 4h and 4j). We found that, assuming additional slip on the antithetic fault or on the low-angle dislocation, the RMS for InSAR data decreases in both cases by ~10–15% and for GPS data by ~7–10% (Table S3 and Figures S12 and S13) with respect to what was obtained modeling only the MGVB main fault system (Figure S9). Both the explored solutions (Figures 4g and 4h) show a main patch of slip located between 2 and 4 km depth, with maximum slip of

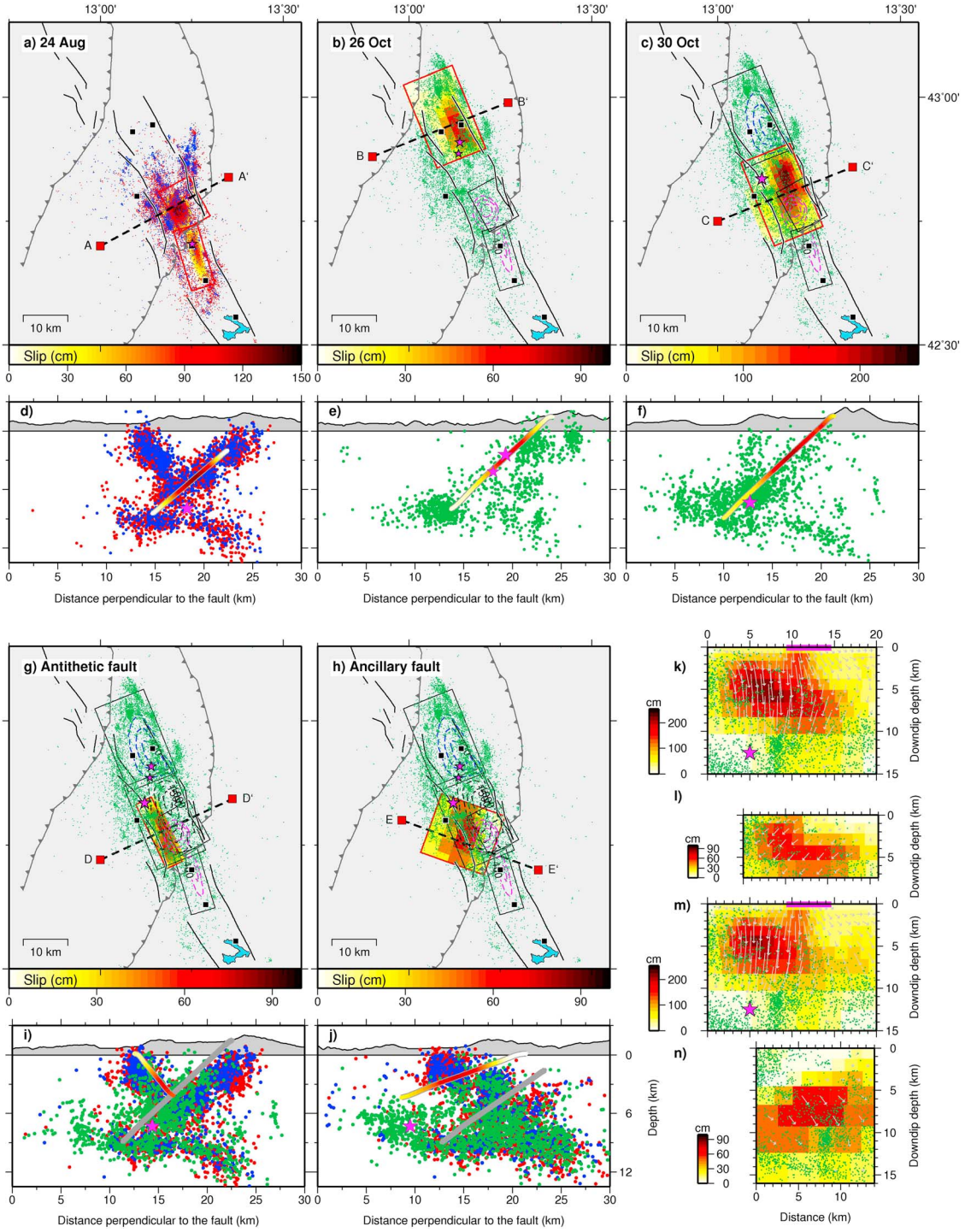

Figure 4. Geodetic model of the 2016 Central Italy earthquake sequence. (a and d) The 24 August Amatrice, (b and e) the 26 October Visso, and (c and f) the 30 October Norcia coseismic slip distributions. Ancillary slip distributions assuming that normal slip occurred either on an (g and i) antithetic fault or on a (h and j) preexisting compressional structure. Seismicity: purple stars indicate the main events; dots are relocated aftershocks (red = between 24 August and 24 September; blue = 25 September and 25 October; green = 26 October and 30 November). (k–n) Slip distributions on the 30 October fault plane (k and m) and on the ancillary dislocations (l = antithetic fault; n = preexisting compressional structure) and relocated aftershocks that occurred within 2 km on each side of the fault plane.

~0.7–0.8 m, equivalent to a M_w ~ 6.1–6.2 earthquake (Table S4). The fact that no large aftershocks occurred around the two hypothesized ancillary faults suggests that the secondary dislocation may have slipped mostly aseismically.

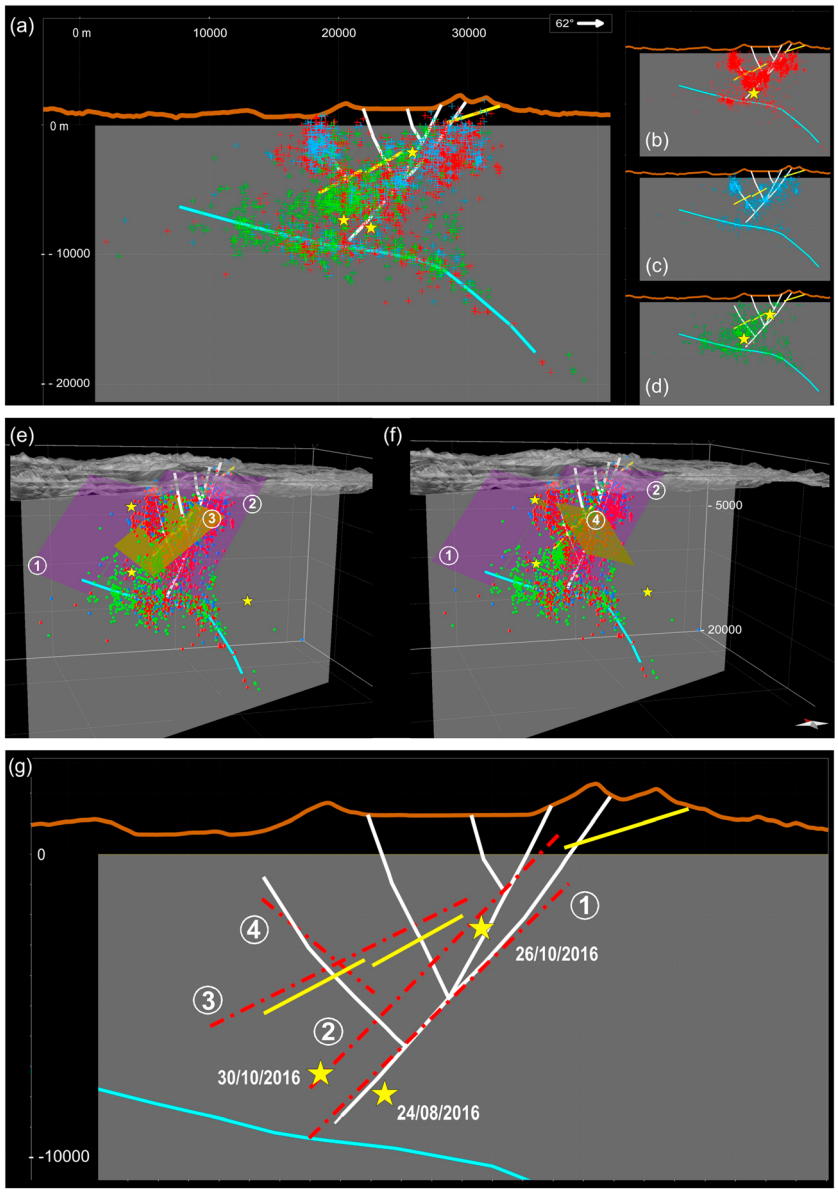

Figure 5. Three-dimensional modeling results and structural sections. Yellow lines are the known tectonic features of the area from *Lavecchia et al.* [2016], while cyan and white lines are from *Lavecchia et al.* [2017]. (a) Earthquake distribution projected on a SW-NE structural cross section (color as in Figure 4); (b–f) 3-D view of the geodetic models (1 = Mount Bove and 2 = Mount Vettore fault planes; 3 = low-angle compressional structure; 4 = antithetic faults), seismicity (yellow stars are the main events), and structural sections; (g) Cross section of proposed models along with structural features.

4. Discussion and Conclusions

The 2016 Central Italy earthquakes represent the largest Italian seismic sequence affecting a continental extensional domain that has been densely observed with modern geodetic measurements. Geodetic data show that the sequence evolved along a main SW dipping normal fault system, relative to the MGVB alignment. The 24 August M_w 6.1 main shock ruptured two distinct segments of this fault system (Figure 4a), corresponding to the northern part of the ~50° SW dipping Mount Gorzano Fault, which was partially activated in its southern portion during the 2009 L'Aquila earthquake [*Chiaraluce et al.*, 2011; *Bigi et al.*, 2013; *Cheloni et al.*, 2014], and to the southern part of the ~40° SW-dipping Mount Vettore Fault, respectively. The main shock occurred, with a bilateral rupture, between these two fault segments, possibly merging into a single SW dipping structure at the hypocentral depth [*Lavecchia et al.*, 2016; *Tinti et al.*, 2016; *Chiaraluce et al.*, 2017].

The 26 October M_w 5.9 Visso event ruptured a northern ~15 km long segment of the MGVB fault system (Figure 4b). This event occurred on a ~ 40° SW dipping fault, with a main patch of slip located in the southeastern part of the plane, supporting the hypothesis of a unilateral northward rupture. The difference between geodetic (M_w 6.1) and seismologic (M_w 5.9) moment magnitude estimates is likely ascribed to an early postseismic contribution.

Finally, the 30 October M_w 6.5 Norcia main shock ruptured the ~20 km long segment that had remained unbroken after the previous large events (Figure 4c). The main shock occurred on the Mount Vettore normal fault, which was only partially activated in its southern portion during the 24 August earthquake. In this case, we found a main patch of slip (with peak slip up to $>$2 m) located at the center of the fault plane (between 3 and 7 km depth). The slip reaches the surface in the area where surface ruptures were observed [*Galadini et al*., 2017].

Our results also indicate that during the 30 October earthquake, an additional dislocation below the Castelluccio plain likely occurred within the sequence, with a retrieved slip equivalent to a M_w ~ 6.1–6.2 earthquake. As regards the nature of this ancillary dislocation, a structural section [*Lavecchia et al*., 2017] across the activated crustal volume and relocated aftershocks [*Chiaraluce et al*., 2017] shows the existence of both antithetic and synthetic faults and of inherited low-angle compressive structures (Figure 5), in agreement with the general tectonic setting of the Central Apennines. In this geological context, the two possible candidates or their combination (Figures S14 and S15) are therefore (1) a NE dipping normal fault antithetic to the MGVB fault system and illuminated by the aftershocks distribution and (2) a preexisting compressional low-angle structure, likely related to a segment of the Sibillini Thrust [*Lavecchia et al*., 2016]. Indeed, by projecting the low-angle ancillary dislocation model along the structural sections, we find a good agreement with the Sibillini Thrust location (Figure 5). Despite that the performed geodetic analysis is unable to discern between the two possible scenarios, the distribution of seismicity suggests the activation of an antithetic normal fault, favoring the assumption that the additional slip may happened on this ancillary structure. On the other hand, the geological context and seismicity pattern do not rule out the hypothesis that also an inherited compressive structure may be reactivated during the sequence. In conclusion, the inversion of geodetic data revealed the progressive activation of four main coseismic asperities during the whole 2016 Central Italy seismic sequence, belonging to the MGVB SW dipping normal fault system, located between the northern termination of the 2009 L'Aquila seismic sequence and the southern termination of the 1997 Colfiorito sequence. Moreover, our results allow us to highlight that some extra slip occurred on a secondary fault structure; this may be related to the activation of a normal fault antithetic to the MGVB main fault system and/or to a preexisting compressional low-angle structure, extensionally active during the seismic sequence. These findings suggest a complex interaction in the activated crustal volume between the main normal fault system and the secondary structures and a partitioning of strain release that may have important implications for the evaluation of the seismic hazard in this sector of the Central Apennines.

Acknowledgments

Most of the figures were made using the GMT software [*Wessel and Smith*, 1998]. This work has been partially funded by the Italian Civil Protection Department, by I-AMICA project (PONa3_00363), and by the EPOS-IP project of the European Union Horizon 2020 Research and Innovation program under grant agreement 676564. As far as authors of the Italian Civil Protection Department (D.D.B., R.G., and M.M.), the views and conclusions contained in this paper are those of the authors, and they should not be interpreted as necessarily representing official policies, either expressed or implied, of the Italian Government. Sentinel-1 data are copyright of Copernicus (2016). ALOS-2 data are copyright of JAXA (2016), and they have been collected through the ALOS-2 AO number P1101002. COSMO-SkyMed data are copyright of ASI (2016), and they have been acquired through a dedicated acquisition plan. The GPS coseismic offsets are provided in the supporting information.

References

Albano, M., M. Saroli, M. Moro, E. Falcucci, S. Gori, S. Stramondo, F. Galadini, and S. Barba (2016), Minor shallow gravitational component of the Mt. Vettore surface ruptures related to M_w 6, 2016 Amatrice earthquake, *Ann. Geophys.*, *59*(5), doi:10.4401/ag-7299.

Atzori, S., I. Hunstad, M. Chini, S. Salve, C. Tolomei, C. Bignami, S. Stramondo, E. Trasatti., A. Antonioli, and E. Boschi (2009), Finite fault inversion of DInSAR coseismic displacement of the 2009 L'Aquila earthquake (central Italy), *Geophys. Res. Lett.*, *36*, L15305, doi:10.1029/2009GL039293.

Bigi, S., P. Casero, C. Chiarabba, and D. Di Bucci (2013), Contrasting surface active faults and deep seismogenic sources unveiled by the 2009 L'Aquila earthquake sequence (Italy), *Terra Nova*, *25*(1), 21–29.

Bignami, C., C. Tolomei, G. Pezzo, F. Guglielmino, S. Atzori, E. Trasatti, A. Antonioli, S. Stramondo, and S. Salvi (2016), Source identification for situational awareness of the August 24th 2016 Central Italy event, *Ann. Geophys.*, *59*(5), doi:10.4401/AG-7233.

Boncio, P. G. Lavecchia, G. Milana, and B. Rozzi (2004), Seismogenesis in Central Apennines, Italy: An integrated analysis of minor earthquake sequences and structural data in the Amatrice-Campotosto area, *Ann. Geophys.*, *47*(6), 1723–1742.

Bonini, L., et al. (2016), Imaging the tectonic framework of the 24 August 2016, Amatrice (central Italy) earthquake sequence: New roles for old players?, *Ann. Geophys.*, *59*(5), doi:10.4401/ag-7229.

Castello, B., G. Selvaggi, C. Chiarabba, and A. Amato (2006), CSI Catalogo della sismicità italiana 1981–2002, versione 1.1. INGV-CNT, Roma. [Available at http://csi.rm.ingv.it/.]

Cheloni, D., et al. (2016), GPS observations of coseismic deformation following the 2016, August 24, M_w 6 Amatrice earthquake (central Italy): Data, analysis and preliminary fault model, *Ann. Geophys.*, *59*(5), doi:10.4401/ag-7269.

Cheloni D., et al. (2014), Coseismic and post-seismic slip of the 2009 L'Aquila (central Italy) M_w 6.3 earthquake and implications for seismic potential along the Campotosto fault from joint inversion of high-precision levelling, InSAR and GPS data, *Tectonophysics*, *622*, 168–185, doi:10.1016/j.tecto.2014.03.009.

Chiaraluce, L., L. Valoroso, D. Piccinini, R. Di Stefano, and P. De Gori (2011), The anatomy of the 2009 L'Aquila norma fault system (central Italy) imaged by high resolution foreshock and aftershock locations, *J. Geophys. Res.*, *116*, B12311, doi:10.1029/2011JB008352.

Chiaraluce, L., et al. (2017), The 2016 Central Italy seismic sequence: A first look at the mainshocks, aftershocks and source models, *Seismol. Res. Lett.*, *88*(3), doi:10.1785/0220160221.

D'Agostino, N. (2014), Complete seismic release of tectonic strain and earthquake recurrence in the Apennines (Italy), *Geophys. Res. Lett.*, *41*, 1155–1162, doi:10.1002/2014GL059230.

Devoti, R., et al. (2017), A combined velocity field of the Mediterranean region, *Ann. Geophys.*, *60*(2), doi:10.4401/ag-7059.

EMERGEO Working Group (2016), Coseismic effects of the 2016 Amatrice seismic sequence: First geological results, *Ann. Geophys.*, *59*(5), doi:10.4401/ag-7195.

Falcucci, E., S. Gori, F. Galadini, G. Fubelli, M. Moro, and M. Saroli (2016) Active faults in the epicentral and mesoseismal Ml 6.0 24, 2016 Amatrice earthquake region, central Italy. Methodological and seismotectonic issues, *Ann. Geophys.*, *59*(5), doi:10.4401/ag-7266.

Galli, P., F. Galadini, and D. Pantosti (2008), Twenty years of paleoseismology in Italy, *Earth Sci. Rev.*, *88*(1–2), 89–117, doi:10.1016/j.earscirev.2008.01.001.

Galvani A., M. Anzidei, R. Devoti, A. Esposito, G. Pietrantonio, A.R. Pisani, F. Riguzzi, and E. Serpelloni (2012), The interseismic velocity field of the central Apennines from a dense GPS network, *Ann. Geophys.*, *55*(4), doi:10.4401/ag-6168.

Galadini, F., E. Falcucci, S. Gori, R. E. Kayen, B. Lingwall, A. Pizzi, A. Di Domenica, P. Zimmaro, and J. P. Stewart (2017), Chapter 2: Seismic source and surface rupture, in *Engineering Reconnaissance Following the 2016 central Italy earthquakes - Version 2*, edited by P. Zimmaro and J. P. Stewart, Geotechnical Extreme Events Reconnaissance Association Report No. GEER-050D, pp. 33–50, doi:10.18118/G6HS39.

Huang, M.-H., E.J. Fielding, C. Liang, P. Milillo, D. Bekaert, D. Dreger, and J. Salzer (2017), Coseismic deformation and triggered landslides of the M_w 6.2 Amatrice earthquake in Italy, *Geophys. Res. Lett.*, *44*, 1266–1274, doi:10.1002/2016GL071687.

INGV Working Group "GPS Geodesy (GPS data and data analysis center" (2016), Preliminary co-seismic displacements for the October 26 (M_w5.9) and October 30 (M_w6.5) central Italy earthquakes from the analysis of GPS stations, Zenodo, doi:10.5281/zenodo.167959.

Lavecchia, G., et al. (2016), Ground deformation and source geometry of the 24 August 2016 Amatrice earthquake (Central Italy) investigated through analytical and numerical modeling of DInSAR measurements and structural-geological data, *Geophys. Res. Lett.*, *43*, 12,389–12,398, doi:10.1002/2016GL071723.

Lavecchia, G., G.M. Adinolfi, R. De Nardis, F. Ferrarini, D. Cirillo, F. Brozzetti, R. De Matteis, G. Festa, and A. Zollo (2017), Multidisciplinary inferences on a newly recognized active east-dipping extensional system in Central Italy, *Terra Nova*, *29*, 77–89, doi:10.1111/ter.12251.

Liu, C., Y. Zhengm Z. Xie, and X. Xiong (2017), Ruptures features of the M_w 6.2 Norcia earthquake and its possible relationship with strong seismic hazards, *Geophys. Res. Lett.*, *44*, 1320–1328, doi:10.1002/2016GL071958.

Lohman, R. B., and M. Simons (2005), Some thoughts on the use of InSAR data to constrain models of surface deformation: Noise structure and data downsampling, *Geochem. Geophys. Geopsyst.*, *6*, Q01007, doi:10.1029/2004GC000841.

Okada, Y. (1985), Surface deformation due to shear and tensile faults in a half-space, *Bull. Seismol. Soc. Am.*, *75*, 1135–1154.

Pepe, A., P. Berardino, M. Bonano, L. D. Euillades, R. Lanari and E. Sansosti (2011), SBAS-based satellite orbit correction for the generation of DInSAR time-series: Application to RADARSAT-1 data, *IEEE Trans. Geosci. Remote Sens.*, *49*(12), 5150–5165.

Petricca, P., S. Barba, E. Carminati, C. Doglioni, and F. Riguzzi (2015), Graviquakes in Italy, *Tectonophysics*, *656*, 202–214, doi:10.1016/j.tecto.2015.07.001.

Pizzi, A., and F. Galadini (2009), Pre-existing cross-structures and active fault segmentation in the northern-central Apennines (Italy), *Tectonophysics*, *476*(1–2), doi:10.1016/j.tecto.2009.03.018.

Rovida, A., R. Camassi, P. Gasperini, and M. Stucchi (2011), CPTI11, the 2011 version of the Parametric Catalogue of Italian Earthquakes, Milano, Bologna. [Available at: http://emidius.mi.ingv.it/CPTI(2011).]

Scognamiglio, L., E. Tinti, and A. Michelini (2009), Real-time determination of seismic moment tensor for Italian region, *Bull. Seismol. Soc. Am.*, *99*(4), 2223–2242, doi:10.7585/0120080104.

Tinti, E., L. Scognamiglio, A. Michelini, and M. Cocco (2016), Slip heterogeneity and directivity of the M_L 6.0, 2016, Amatrice earthquake estimated with rapid finite-fault inversion, *Geophys. Res. Lett.*, *43*, 10,745–10,752, doi:10.1002/2016GL071263.

Wessel, P., and W. H. F. Smith (1998), New improved version of the generic mapping tools released, *Eos. Trans. AGU*, *79*(47), 579–579, doi:10.1029/98EO00426.

Williams, C. A., and G. Wadge (1998), The effects of topography on magma chamber deformation models: Application to Mt. Etna and radar interferometry, *Geophys. Res. Lett.*, *25*(10), 1549–1552, doi:10.1029/98GL01136.